

Master's thesis

2019

Hauk-Morten Heimlund Lykke

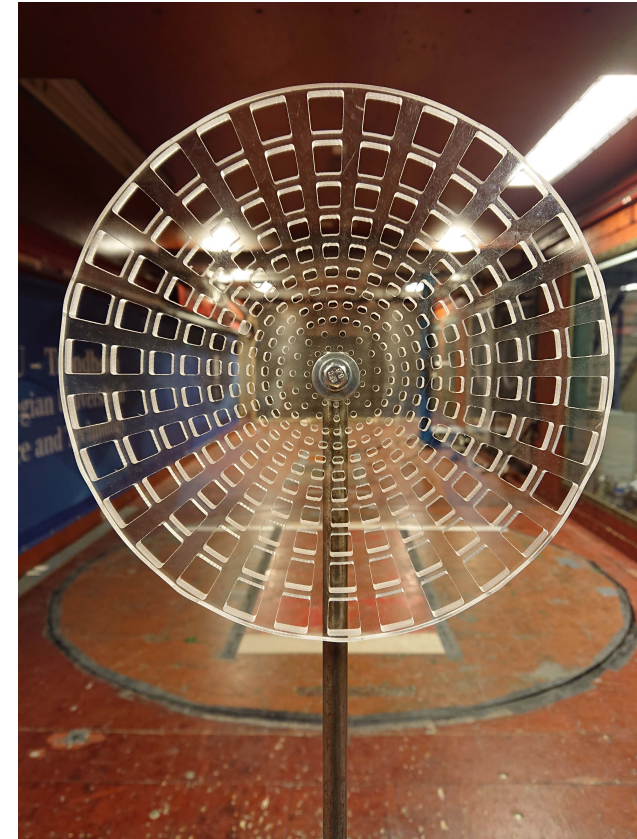
Master's thesis

**NTNU**  
Norwegian University of  
Science and Technology  
Faculty of Engineering  
Department of Energy and Process Engineering

Hauk-Morten Heimlund Lykke

The effect of turbulence and blockage orientation on the near-field of porous disks

February 2019







Norwegian University of  
Science and Technology

# The effect of turbulence and blockage orientation on the near-field of porous disks

**Hauk-Morten Heimlund Lykke**

Mechanical Engineering

Submission date: February 2019

Supervisor: Robert Jason Hearst

Co-supervisor: Magnus Kyrkjebø Vinnes

Norwegian University of Science and Technology  
Department of Energy and Process Engineering



---

# Abstract

Wind tunnel experiments have been conducted with a solid disk and two different porous disks, with identical solidity, placed in flows with two different turbulence intensities at a Reynolds number of  $Re = 110\,000$ . One of the porous disks is a perforated plate, the other is made of wire mesh. Velocity measurements have been performed in the wakes of the three objects, and high order statistics have been compared. The objective was to quantify characteristics of the near wakes and further to determine how and to what extent the shape of a porous disk affects its wake. In agreement with earlier studies, the decay rate of the wake half width ( $\delta$ ) was found to increase, and centre-line velocity deficit ( $U_S$ ) decreased for all disks when subjected to incoming turbulence. However, the onset of the wake recovery was found to be delayed for the mesh disk, which is surprising. The mesh disk forms a narrow and separated annular shear layer at the disk edge as opposed to the very turbulent region behind the entire perforated disk, which more closely resembles that of the solid disk. The incoming turbulence promotes the onset of self-similarity for all disks. The velocity skewness and kurtosis were found to decrease in magnitude for increased incoming turbulence intensity. The solidity and overall topology of a perforated disk are known to be important in determining drag and recirculation in the wake, however we have found the differences between a mesh disk and a perforated disk to be at least as big.

# Sammendrag

Vindtunnel-eksperimenter har blitt gjennomført med en solid disk og to ulike porøse disker med identisk soliditet plassert i strømninger med to forskjellige turbulens-intensiteter med et Reynoldstall på  $Re = 110\,000$ . En av de porøse diskene var en perforert plate, den andre var laget av trådduk. Hastighetsmålinger har blitt gjennomført i dragsuget av de tre objektene, og høyere ordens-statistikk har blitt sammenlignet. Målet var å kvantifisere karakteristika av de nære dragsugene og å bestemme hvordan og i hvilken grad formen til en porøs disk påvirker dragsuget. I overenstemmelse med tidligere studier, har raten av tilbakegang for dragsug-halvbredden  $\delta$  blitt funnet til å stige, og hastighetsfallet langs senterlinjen  $U_S$  har sunket for alle diskene når de utsettes for incommende turbulens. Gjenopprettingen av dragsuget bak trådduk-diskene har vist seg å forsinkes av turbulensen, noe som er overraskende. Trådduk-diskene former et smalt og separat ringformet skjærlag langs kanten av disken, i motsetning til den sterkt turbulente regionen bak hele den perforerte disken, som ligner mer på dragsuget til den solide disken. Den innkommende turbulensen fremskynder begynnelsen på egenlikhet for alle diskene. Den statistiske skjevheten og kurvaturen har blitt funnet å minke i størrelse ved høyere incommende turbulens. Soliditeten og formen til en perforert disk er kjent å påvirke drag og resirkulasjon i dragsuget, imidlertid har vi funnet at forskjellene mellom en trådduk-disk og en perforert disk er minst like store.



# Preface

This project was suggested to me by my supervisor R. Jason Hearst as an interesting alternative to my original plans. Choosing this project is one of my better decisions as a student. It has been incredibly interesting, and even more challenging. I have learned incredibly much. I have several times had the feeling I might be in over my head, both regarding amount of work, knowledge and intelligence, but it is finally coming together after all. This task would simply not have been possible without all the help, guidance and constant availability of Jason and Magnus. I could not have managed all the lab hours and the problem solving without both of you, and for that I am incredibly grateful. I am grateful to the technicians who just fix things whenever they don't fit or work, and for answering all of the beginner's questions in the workshop. I would like to thank my parents for helping me with proofreading, giving feedback and being supportive. And finally I would like to thank my wife Therese, and my son Falk, for bearing with me despite my absentmindedness, and for my recurring inability to go to bed at sensible hours. Therese, I owe you a lot of work at home. Your support, feedback, love and your ability to pull me back to the moment and enjoy life makes all the difference in the world, and I hope you realize how much that means to me.

*Trondheim, 30. Januar 2019  
Hauk-Morten Heimlund Lykke*



# Table of Contents

<b>Abstract</b>	<b>i</b>
<b>Sammendrag</b>	<b>i</b>
<b>Preface</b>	<b>iii</b>
<b>Table of Contents</b>	<b>v</b>
<b>1 Introduction</b>	<b>1</b>
1.1 Solid disk wakes . . . . .	1
1.2 Porous disk wakes . . . . .	2
1.3 The effect of incoming turbulence . . . . .	4
1.4 Research objectives . . . . .	4
<b>2 Experimental setup</b>	<b>7</b>
2.1 Test facility and grid layout . . . . .	7
2.2 Hotwire anemometry . . . . .	7
2.3 Disks . . . . .	9
2.4 Sampling Procedure . . . . .	9
<b>3 Results and discussion</b>	<b>13</b>
3.1 Mean velocity profiles . . . . .	13
3.2 Turbulence intensity . . . . .	13
3.3 Effect of turbulence . . . . .	13
<b>4 Conclusion</b>	<b>25</b>
<b>Bibliography</b>	<b>25</b>
<b>Appendix</b>	<b>31</b>



Chapter **1**

# Introduction

The flow behind a disk is a canonical problem. It is easy to reproduce, and many different objects can be approximated by a disk. Among other bluff bodies, it is especially useful because of its ability to model anything rotating, and for such applications, porous disks are even more relevant. They are more similar to rotating objects than solid disks where the swept area is larger than the frontal area, because they let some of the flow pass through. The wake is interesting to understand for two reasons. The first is that the object creating the wake is highly affected by the wake. For example, an square bar and a cylinder create very different wakes, and as a consequence they are subjected to very different forces. The other reason is that any object placed in a wake experiences a very particular kind of flow. The latter is important, because the wake is often present very far downstream of the object creating it. A phenomenon that is particular to jets and wakes, is what is known as self-similarity. This phenomenon is basically that past a certain point downstream, some important parameters of a jet or a wake will cease to evolve, and will maintain a certain structure, it will become "self-similar". The following subsections will try to summarize what is known, and what is interesting to investigate further within this topic.

## 1.1 Solid disk wakes

The wake behind solid disks has been extensively investigated for at least half a century (Uberoi & Freymuth 1970, Tennekes & Lumley 1972, Johansson et al. 2003, Rind & Castro 2012*a,b*). Although a few recent studies investigate wakes in a turbulent incoming flow (Myers & Bahaj 2010, Rind & Castro 2012*a*, Blackmore et al. 2013), most of the research has been concerned with a disk in a laminar flow (Rind & Castro 2012*a*). However, since the vast majority of real flows are turbulent, the characteristics of a wake occurring in a turbulent flow are also important. Sforza & Smorto (1981) postulated that the wake recovery will increase as a result of increased incoming turbulence by increasing the mixing rate between the freestream and the wake. This was later confirmed by Myers & Bahaj (2010), Wu & Porté-Agel (2012), Rind & Castro (2012*a*), Blackmore (2013) and Nedic (2013).

It is commonly believed that axisymmetric turbulent wakes sooner or later reach a universal self-similar state (Redford et al. 2012), as first hypothesized by Townsend (1980). The classical behaviour described by the far-field self-similarity solution for axisymmetric, turbulent wakes

in a laminar incoming flow is that the wake half width  $\delta$  increases with  $x$  such that

$$\delta \propto x^{1/3} \quad (1.1)$$

and the centre-line velocity deficit  $U_s$  decreases with  $x$  as

$$U_s \propto x^{-2/3} \quad (1.2)$$

as shown by Tennekes & Lumley (1972), where  $U_s = U - U_\infty$  where  $U$  is the local mean velocity and  $U_\infty$  is the freestream velocity. The half-width of the wake ( $\delta$ ) is here, as commonly, defined as the radial position where the velocity deficit is half of its maximum (Rind & Castro 2012a). Uberoi & Freymuth (1970) found that the self-similar behaviour appears first at  $x > 50D$ , where  $D$  is the disk diameter. A direct numerical simulation (DNS) study performed by Redford et al. (2012) found that although such a universal state can appear, two wakes created by different inlet conditions will not actually become similar before a downstream position on the order of  $\mathcal{O}(5000D)$ , which occurs very rarely in practice. This finding suggests that the wakes from solid disks and porous disks behave quite differently, and these differences have a lasting influence within a realistic flow development distance. As a consequence, there is a need to improve the understanding of the wakes of porous disks and if the way their solidity is oriented has a significant impact on the flow development.

Before we proceed, some relevant parameters will be defined. Turbulence intensity is here defined as  $u'/U$  where  $u'$  denotes the root mean square of velocity fluctuations ( $u$ ) around the temporal local mean velocity  $\bar{U}$ , giving  $u = U - \bar{U}$ . The skewness ( $S$ ) and kurtosis (also called flatness) ( $K$ ) which are defined as

$$S = \frac{\overline{u^3}}{(\overline{u^2})^{3/2}}, \quad (1.3)$$

$$K = \frac{\overline{u^4}}{(\overline{u^2})^2} \quad (1.4)$$

are both scaled with the variance of the velocity fluctuations  $u$ ,  $\overline{u^2}$  to become dimensionless. The skewness  $S$  is a measure of asymmetry of the probability distribution of  $u$ , and the kurtosis  $K$  is a measure of the likelihood of high magnitudes of the velocity fluctuations. The skewness in this context also represents a value of isotropy, where a low skewness indicates high isotropy (Mohamed & Larue 1990).

When studying wakes, it is useful utilize the similarity scalings,  $f$  and  $\eta$ , given by Pope (2000) as

$$f = \frac{U_\infty(x) - U(r, x)}{U_s(x)}, \quad \eta = \frac{r}{\delta(x)} \quad (1.5)$$

in order to investigate whether the shape of the mean velocity exhibits a dependency of the streamwise coordinate  $x$ .

## 1.2 Porous disk wakes

Porous disks are other wake generators of interest. They represent physical actuator disks, and actuator disks are used in many applications for simplifying flows and flow calculations. Many

numerical computations of turbines are for instance done using variants of actuator disk models (Aubrun et al. 2013, Rind & Castro 2012b, Wu & Porté-Agel 2012). Porous disks are also used in scale model research of wind turbines (Aubrun et al. 2012, Blackmore et al. 2013), and they are practical for experiments because they are much easier to manufacture than fully functioning turbines, while still yielding useful results (Aubrun et al. 2013, Bossuyt et al. 2017).

Higuchi et al. (1998) performed particle image velocimetry (PIV) experiments in the near wake of porous disks with annular slots, the disks simulating ribbon parachutes. They found that the flow through the slots shaped jets that would, depending on the spacing between slots, merge and form high-momentum regions that displaced the reverse-flow region typically found behind solid disks. These regions were deemed more axisymmetric than those of the solid disk, and they were persistent downstream. It is important to note that the porous disks used by Higuchi et al. (1998) had an opening in the center (vent) that previous experiments showed made a large difference concerning axisymmetry and reversed flow, since the center jet was not deflected. Theunissen & Worboys (2019) later performed PIV experiments with disks with 4-6 annular holes with varying hole diameter, and confirmed the merging of jets for Reynolds numbers up to  $Re = 125\,000$  for small hole spacing. They also found that if the distance between the annular holes and the perimeter of the disk was small enough, the jets merged with the annular shear layer. Cannon (1993) performed flow visualizations with porous disks and solid disks. They used mesh disks (also known as gauze disks) and investigated a downstream region of up to 185 momentum lengths, or roughly  $90D$ . Cannon (1993), Higuchi et al. (1998) and Theunissen & Worboys (2019) only performed experiments with a laminar incoming flow. It has further been shown that an increase in the solidity (the ratio of the solid area to frontal area) of a porous disk increases the rate of the velocity deficit decay and decreases the rate of the wake width expansion (Cannon 1993, Higuchi et al. 1998, Myers & Bahaj 2010, Blackmore et al. 2013, Theunissen & Worboys 2019).

Aubrun et al. (2013) performed hotwire experiments in order to compare the wake behind a porous disk with that of a rotating wind turbine. They also performed analysis of the velocity skewness and kurtosis of the wakes. The experiments were conducted at streamwise positions of  $x = 0.5D$  and  $x = 3D$  with a sample length of 180 s and a sampling frequency of 6 kHz. A wire mesh disk represents a grid turbulence generator. Such grids were shown by Mohamed & Larue (1990) to give a turbulence intensity that decays with a power law with an exponent that is Reynolds number independent for  $Re_M = 6000$  to  $68\,000$ , where  $M$  is the mesh size. It was based on this argument that Aubrun et al. (2013) chose to use a mesh disk for their investigations. The experiments by Aubrun et al. (2013) were conducted with two different incoming flow conditions at a  $Re = 70\,000$ , one with decaying grid turbulence and one with a simulated atmospheric boundary layer. The grid turbulence case had a turbulence intensity of  $u'_\infty/U_\infty = 4\%$ . At  $x = 3D$ , the velocity deficits of the disk and the turbine were identical, and the turbulence intensity and skewness had reached quite similar states. The statistical error for the skewness and kurtosis for the grid turbulence case had a reported maximum of 11.3% and 45.3% respectively. The turbulence in the wake of the porous disk was found to be produced primarily in the annular shear layer caused by the velocity deficit, and not so much by the grid itself. Thus, the third- and forth-order velocity moments were not well converged in these studies, and there is little other documentation on these moments behind porous disks.

Camp (2018) performed stereoscopic PIV experiments with an array of stationary porous disks and compared it to an array of rotating turbines. The investigations included mechanisms of transport of the mean kinetic energy within the wakes. She found that the largest differences between the two setups were in the spanwise mean velocity in the near wake. It was deemed

that porous disks adequately represents the transport of mean kinetic energy from a rotor in the far wake, where rotation is less important. Other relevant specifics of their experiments are unfortunately not available yet.

### 1.3 The effect of incoming turbulence

Myers & Bahaj (2010) investigated the effect of incoming turbulence on mesh disks with varying incoming turbulence intensity and disk solidity, and they found that neither changes the wake recovery notably. It is important to note that the turbulence was induced by channel bed roughness modelling a seabed, and thus the integral length scale  $l$  of the turbulence was an order of magnitude smaller than the disk diameter. The turbulence integral scale is here defined as the approximate size of the largest turbulent eddies containing the most energy. This experiment was also conducted in an open water channel of a size that made gravitational effects impossible to ignore, and the turbulence intensity was not reported.

Rind & Castro (2012a) performed experiments in order to determine the effect of incoming turbulence on the axisymmetric wake of a solid disk. They measured velocities for downstream positions  $65 < x/D < 115$ . In particular, they showed that an increased incoming turbulence intensity and length scale increases the wake momentum deficit and the far wake's velocity decay rate, in addition to preventing the appearance of self-similarity. The incoming turbulence caused a turbulence structure in the wake that gradually evolved into that of the incoming turbulence, where the turbulence normal stresses became constant with radius  $r$  and eventually equal to the incoming stress levels. For the control case with a laminar incoming flow, they confirmed the self-similar behaviour described by Tennekes & Lumley (1972). Rind & Castro (2012b) later performed a DNS of a time developing axisymmetric wake. The wake generator was not actually included in the simulation, they used measurement results acquired from Chevray (1968) as an inlet condition. The Reynolds-number for the simulation was  $Re = U_S \delta / \nu = 10\,000$  based on the maximum velocity deficit  $U_s$  and the wake half-width  $\delta$  at  $x/D = 1$ , which makes the  $Re_D = U_\infty D / \nu > 10\,000$ . The DNS study reported the same findings as mentioned from their earlier experiments (Rind & Castro 2012a).

Blackmore et al. (2013) placed disks perforated with circular holes in varying incoming turbulence, and initiated the turbulence with turbulence grids. They measured turbulence intensity and varied integral length scales  $l$  for  $Re = 38\,000$  to  $52\,000$ . They found that the disks experienced a significant increase in drag with higher turbulence intensity up to a turbulence intensity of around 13%, where it converged. The drag was at a minimum when  $l/D \approx 0.5$  whilst the drag increased for larger and smaller length scales. España et al. (2012) investigated the effect of large scale turbulence on wake meandering, and found a low frequent meandering movement in the wake that could not be attributed to periodic vortex shedding.

While the asymptotic behaviour of the wakes are interesting, many flows inside wakes often occur much closer in practice. Two examples of relevant applications today are wind- and tidal turbines, and wind turbines are typically placed with a streamwise spacing of 7-10 rotor diameters (Wu et al. 2019).

### 1.4 Research objectives

Of the studies mentioned, only Aubrun et al. (2013) investigated the high order statistics of the wakes. A review of the literature identifies that incoming turbulence plays a role in the wake

development of solid and porous disks, but it is not clear how the shape of a porous disk affects the wake. It is known that the turbulence enhances momentum transport into the wake of a solid disk, but it is unclear how this holds for porous disks where some of the turbulence is allowed to pass through the disk. If porous disks are to be used as model turbines, understanding the characteristics of their wakes, and particularly the near wakes, in realistic flow conditions is of great importance. Moreover, given that any interaction likely starts at the shear layer on the edge of the disk where intermittency is high, the high-order statistics are particularly interesting in that region, as they are indicators for these intermittent reactions. This study aims to investigate wakes in similar incoming conditions as Rind & Castro (2012*a,b*) and Aubrun et al. (2013), with porous disks similar to the ones used by Aubrun et al. (2013) and Higuchi et al. (1998). The intention is to expand the knowledge of such flows with Reynolds numbers an order of magnitude higher than most previous studies (Higuchi et al. 1998, Cannon 1993, Redford et al. 2012, Rind & Castro 2012*a,b*, Bossuyt et al. 2017), as flows in practical applications often operate in much higher Reynolds numbers. The objective is to quantify up to fourth order statistics (kurtosis) of wakes behind three different kinds of disks, two of them porous with similar solidity and different shape. As such, hot-wire measurements were performed in the wakes of the disks for two different incoming turbulence intensities. The turbulent integral scales will not be discussed in detail, as using turbulence grids with large length scales while maintaining a sufficiently homogenous incoming flow was not possible due to space limitations.



# Chapter 2

## Experimental setup

### 2.1 Test facility and grid layout

The experiments were conducted in the large closed-circuit wind tunnel at the Norwegian University of Science and Technology. The test section in the tunnel measures  $12\text{ m} \times 1.8\text{ m} \times 2.7\text{ m}$ . The ceiling in the tunnel is adjustable, and the angle of it is set to create an approximately zero-pressure-gradient along the tunnel length. This allows for a homogenous mean velocity along the test section. The tunnel is equipped with a traverse mechanism that enables automated positioning of measurement probes inside the tunnel. The range of the traverse in the horizontal direction is  $\pm 750\text{ mm}$ , so the distance between the outermost possible position and the wall is  $\sim 600\text{ mm}$  or in this case  $3D$ . The measurements were conducted with two different turbulence intensities at  $Re_D \approx 110\,000$ . A schematic of the setup is shown in Figure 2.1. The low turbulence intensity setup had a mean turbulence intensity of  $u'_\infty/U_\infty = 0.36\%$  in the empty tunnel. The setup consisted of the mesh screen shown in Figure 2.2a at the inlet with wire thickness  $t_1 = 0.6\text{ mm}$ , meshlength  $M_1 = 2.49\text{ mm}$  and solidity  $\sigma_1 = 35.4\%$ . The high turbulence intensity was created with a biplanar wooden grid at the inlet (Figure 2.2b) consisting of square bars with thickness  $t_2 = 46\text{ mm}$ , meshlength  $M_2 = 242\text{ mm}$  and solidity  $\sigma_2 = 34.4\%$ . This was placed  $5.4M_2$  upstream of the fine mesh. The average turbulence intensity was measured to be  $u'_\infty/U_\infty = 4.13\%$  across the test section at  $x = 0$  with the high turbulence intensity setup. This was measured at the streamwise position of the disk, but in absence of it. A power law fitted to the decay of the turbulence intensity downstream of the fine mesh results in a decay rate of  $u' \propto x^{-1}$ . The fine mesh was located a distance of  $\sim 100M_1$  upstream of the disk to ensure that the turbulence had sufficient time to evolve and homogenize before meeting the disks.

### 2.2 Hotwire anemometry

The velocity measurements were conducted simultaneously with three single-wire hot-wires (Dantec type 55P11). The wires were operated in constant temperature mode with an overheat of  $\alpha = 0.8$  using a Dantec Streamline Pro anemometer. Two different hotwire setups were used. The first consisted of two wires mounted 80 mm apart in a holder made of a rectangular aluminum block, the supports were mounted in drilled holes with set screws. Between the hotwires the following were placed: a pitot-static tube, a Dantec resistance temperature detector (RTD) probe and an Omega T-type thermocouple. The second setup is shown in Figure 2.3 and

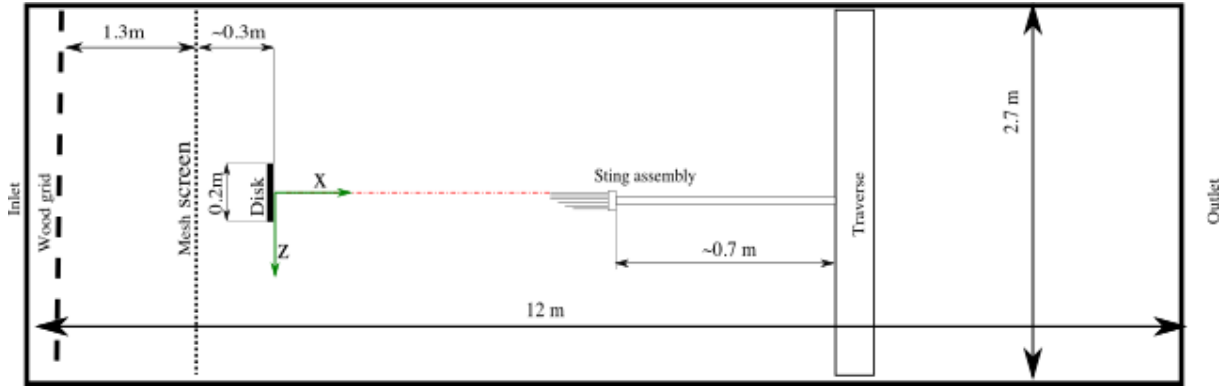


**Figure 2.1:** Schematic of the high TI setup seen from above. The laminar setup is without the first wooden grid. Not to scale.



**Figure 2.2:** Screens used. The wire mesh screen is shown in (a) and the high turbulence grid is shown in (b).

consisted of three wires with 20 mm spacing, with the remaining probes placed beside the hotwires. The probe holder was mounted to the end of a sting assembly, which has a length of approximately 700 mm. This was mounted to the traverse as shown in Figure 2.4. The pitot-static tube was connected to a pressure transducer, and all signals were acquired using a National Instruments NI-cDAQ 9178 (DAQ). The hotwire outputs from the anemometer were connected to a NI 9215 module, and the temperature output from the anemometer along with the pressure transducer were connected to another NI 9215 module in the DAQ. The T-type thermocouple was connected to a NI 9210 module, and another K-type thermocouple placed at the inside wall of the tunnel was connected to a NI 9215 module. The temperatures read from the thermocouples normally read just above and below the temperature given by the RTD, which is the most accurate. Temperature drift was corrected using the temperatures from the RTD, by the approach of Hultmark & Smits (2010).

In order to minimize the impedance from the cables, the chosen cables were short enough that the anemometer had to be placed inside the wind tunnel. The anemometer was placed downstream of the traverse for all scans, and although the center of the wake was found to shift slightly to the negative  $z$ -side for all disks far downstream, the difference is small, no more than



**Figure 2.3:** The probe holder seen from above. From the top: Hotwires 1, 2 and 3, the pitot-static tube, the T-type thermocouple and the RTD.

0.8° or 1.4% for the worst case. The relevant calculations will be further discussed in section 3.

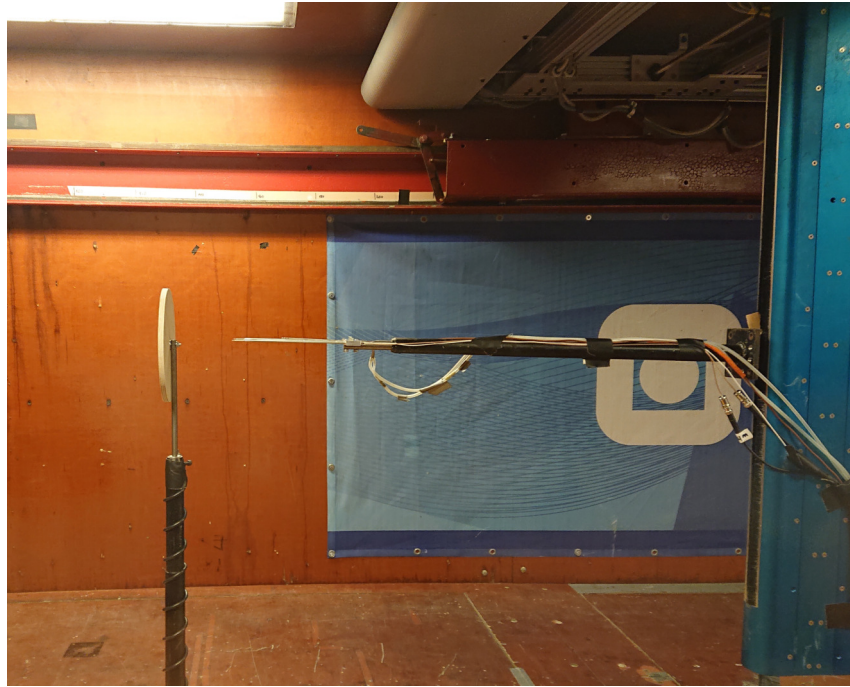
The background flow was measured in order to account for inhomogeneity in the wind tunnel, the homogeneity was found to lie within ±1.25% crosswise in the tunnel and ±1.02% streamwise, as shown in Figure 2.5 and Figure 2.6.

## 2.3 Disks

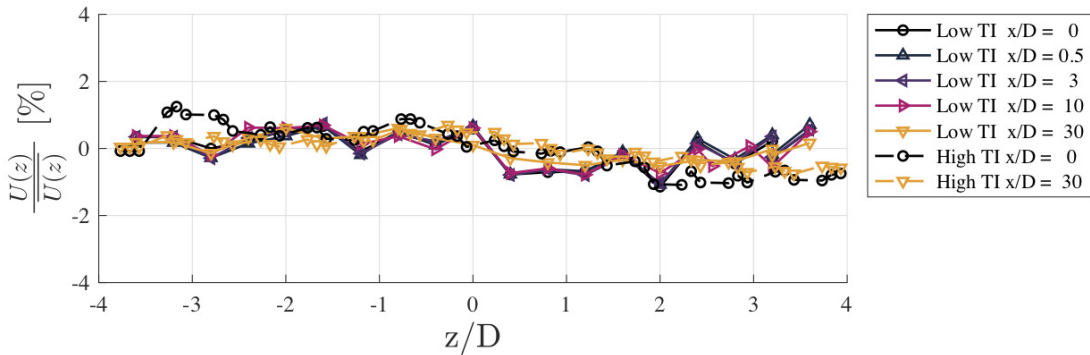
The disks used are all circular with a diameter of  $D = 200$  mm. The solid disk (SD) is made of plywood and has a thickness of 19 mm. The first porous disk (Wire Disk for simplicity, WD), shown in Figure 2.7 is made of a mesh of weaved steel wire with a wire thickness 0.8 mm and solidity  $\sigma = 57\%$ . The disk was mounted to a solid steel tower with a  $\sim 10$  mm diameter. The second porous disk was designed to have the same solidity as that of the WD, and is made of acrylic plastic (Acrylic Disk, AD) shown in Figure 2.8. It has a thickness of 6.5 mm and machined azimuthal slots. The outer region has 30 azimuthal columns and 9 concentric rows of quasi-rectangular filleted holes with 3 mm spacing radially, with two concentric circles of circular holes in the center, a schematic is shown in Figure 2.8. It is fastened to a tower with a nut and bolt and so the center is solid in the experiments.

## 2.4 Sampling Procedure

As the incoming flow was shown to be roughly homogeneous and the disk wakes were expected to be symmetric, measurements were performed with high resolution on one side of the wake, and lower resolution on the other (to check the symmetry). The region behind each disk experiencing changes in either velocity, turbulence intensity, skewness or kurtosis were identified in preliminary tests. Within these regions, a spacing of 10 mm between measurement points was used. Outside of these regions, the maximum spacing was 50 mm on the high resolution side and 160 mm on the low resolution side. The sampling time inside the wake on the high resolution side was 360s, and the minimum sampling time outside the wake and on the low resolution side was 200s.



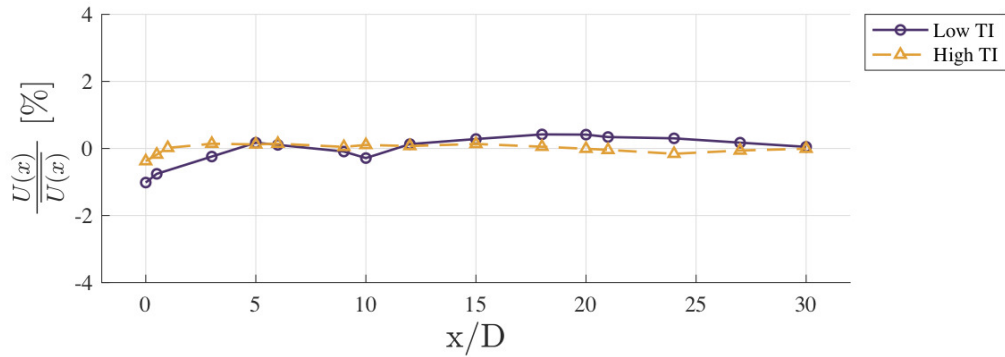
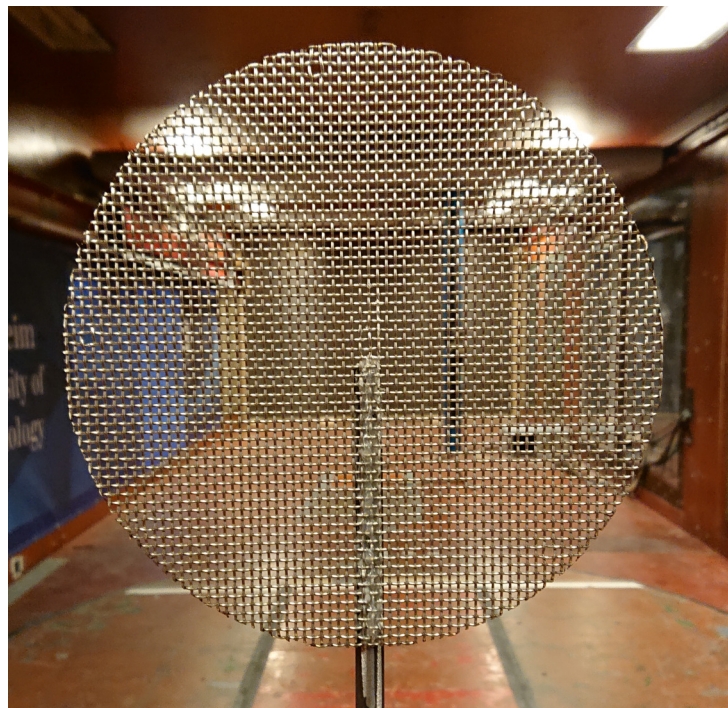
**Figure 2.4:** The setup used in the experiments, here shown with the solid disk mounted. Note the helical cable around the tower in order to break up vortex shedding by the holder.



**Figure 2.5:** Cross stream homogeneity of the tunnel.

Only the mean values of the thermocouples, the pitot-static tube and the RTD were used. Thus, the sampling frequencies of those were set lower than that of the hotwires to limit storage space. A frequency of 1.0 kHz was used for the thermocouples, and 2.0 kHz for the pitot-static tube and the RTD. The hotwire signals were acquired with a frequency of 30 kHz. This frequency was determined by first sampling with a much higher frequency and then estimating the Kolmogorov frequency by examining the power spectral density function of a signal acquired in the most turbulent part of the wake. This is discussed in more detail in the appendix. All signals were then filtered by an analog lowpass filter in the anemometer frame at a cut-off frequency of 10 kHz. After acquisition, the signals were then filtered with a digital Butterworth lowpass filter with the same cutoff frequency.

All hotwires were calibrated at the beginning and the end of each day. At least 12 velocities were used for each calibration. The velocities were normalized against each other in order to compensate for inter-wire drift. Additionally, during most scans one or more positions were

**Figure 2.6:** Streamwise homogeneity.**Figure 2.7:** The wire mesh disk (WD).

deliberately acquired with each wire so that the relative drift could be assessed. Due to the inter-wire drift, the freestream velocity  $U_\infty(x)$  was computed as the average of the mean velocities at the six outermost sampling positions.

The wake was found to shift slightly to the side. The self-similarity properties  $\eta, f, U_s$  and  $\delta$  have therefore been calculated relative to the center of the actual wake instead of  $z = 0$ . Uncertainties are calculated based on the "bootstrap"-idea of Benedict & Gould (1996), but instead of drawing the segments randomly, each segment consists of as many independent points as possible. The number of segments used thus equals the spacing. This way, the entire sample is used for the uncertainty calculation.

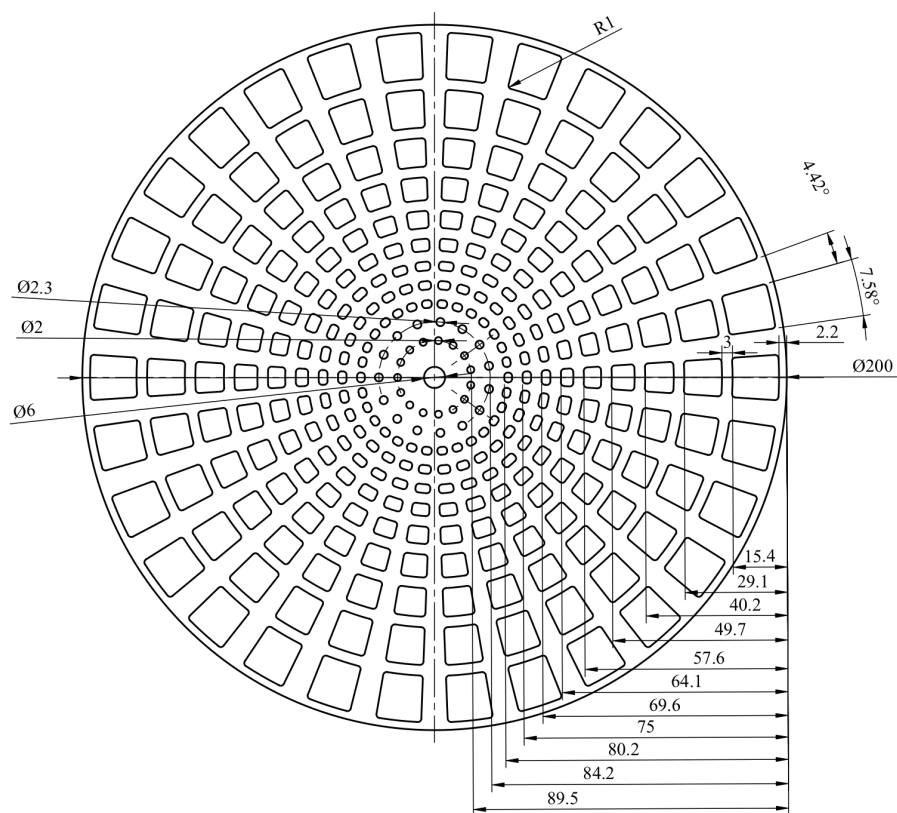


**Figure 2.8:** Schematic of the acrylic disk (AD). Length units in mm, angular units in degrees.

# Chapter 3

## Results and discussion

### 3.1 Mean velocity profiles

The mean velocity profiles of the experiments are given in Figure 3.1 and Figure 3.2. A first look at the two reveals that the velocity deficit is much higher in the near field of the AD than the WD, and that the WD wake, while initially weaker, widens significantly slower than the other two. It is clear that the shape of the disk is important, since the solidity is the same for the two, and this is in agreement with the findings of Theunissen & Worboys (2019).

### 3.2 Turbulence intensity

It is evident from Figure 3.3 that the turbulence production occurs mostly at the annular shear layer, because this is where the mean velocity gradient is the largest. The wake of the WD forms a distinct annular shear layer that does not meet in the center before  $x = 10D$  for the laminar case and  $x = 5D$  for the turbulent case. Aubrun et al. (2013) found the same for their mesh disk, and although the highest turbulence intensity occurs in the same location for the disks, the turbulence intensity in the center of the wake is higher by a factor of  $\sim 4$  for the AD than the WD. For the AD, the annular shear layer merges faster, and the velocity deficit forms an approximate Gaussian shape much sooner than for the WD. The WD also has a local peak of turbulence intensity in the center that the other two disks do not have. This can be attributed to the edge of the tower, which does not go past the disk center, in contrast to the tower of the AD, which is covered by the disk. Cannon (1993) found that recirculation zones appeared for mesh disks with solidities exceeding some critical value between 50% and 60%. Since the velocity gradient changes direction in the shear layer at  $x = 0.5D$  and  $x = 1D$ , it seems possible that there could be a recirculation zone there for the SD and the AD.

### 3.3 Effect of turbulence

The most obvious effect of the higher incoming turbulence on the turbulence intensity in the wakes is that the turbulence decays more rapidly behind the disk, but this is only the case for the SD and the AD. The peak turbulence intensity is virtually unchanged for those. For the WD, the turbulence intensity nearly doubles in the shear layers.

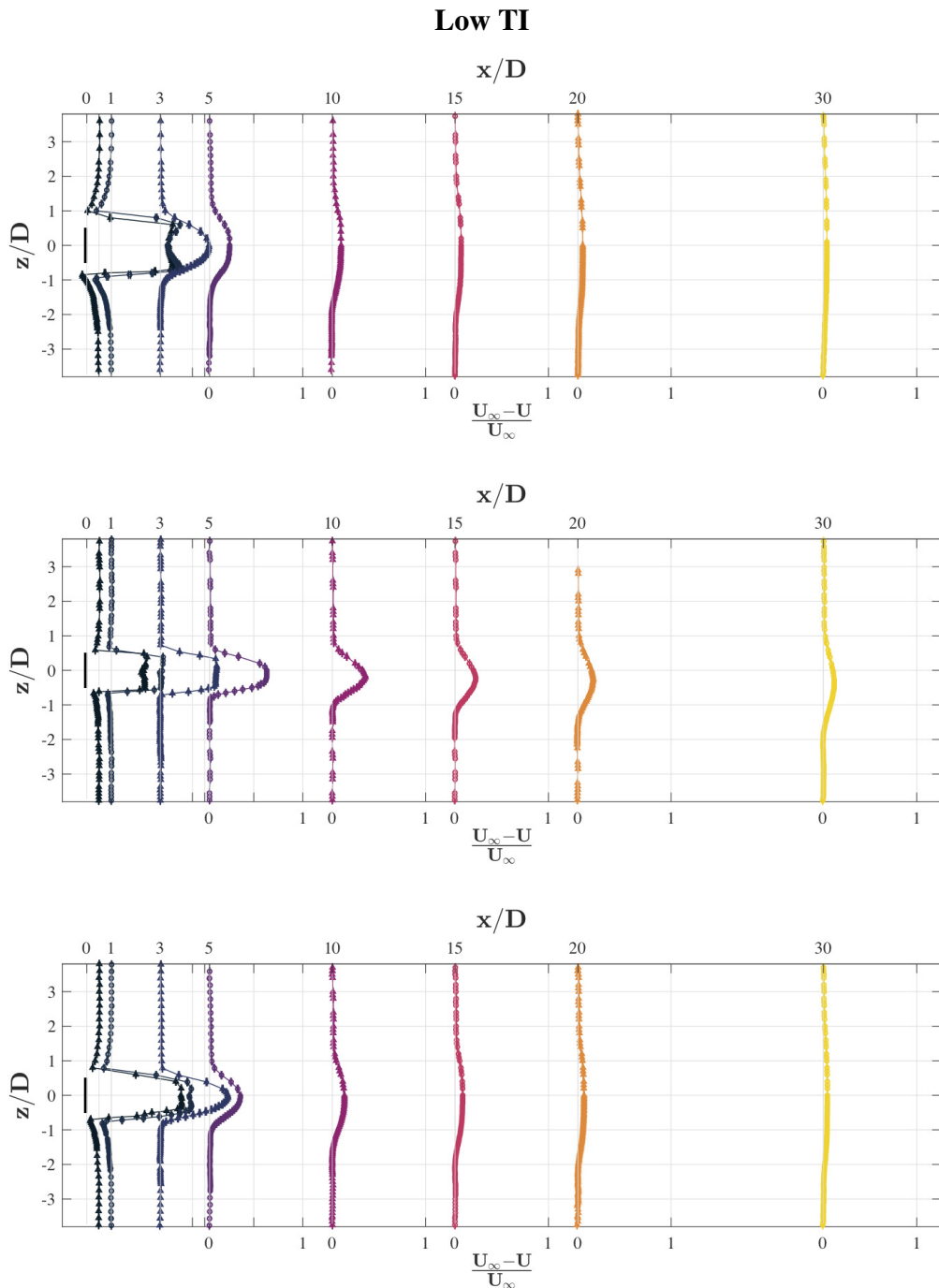


**Figure 3.1:** Mean velocity deficit, an overview of the measurements taken for the laminar case. From the top: SD, WD and AD measurements. Errorbars indicate statistical uncertainty.

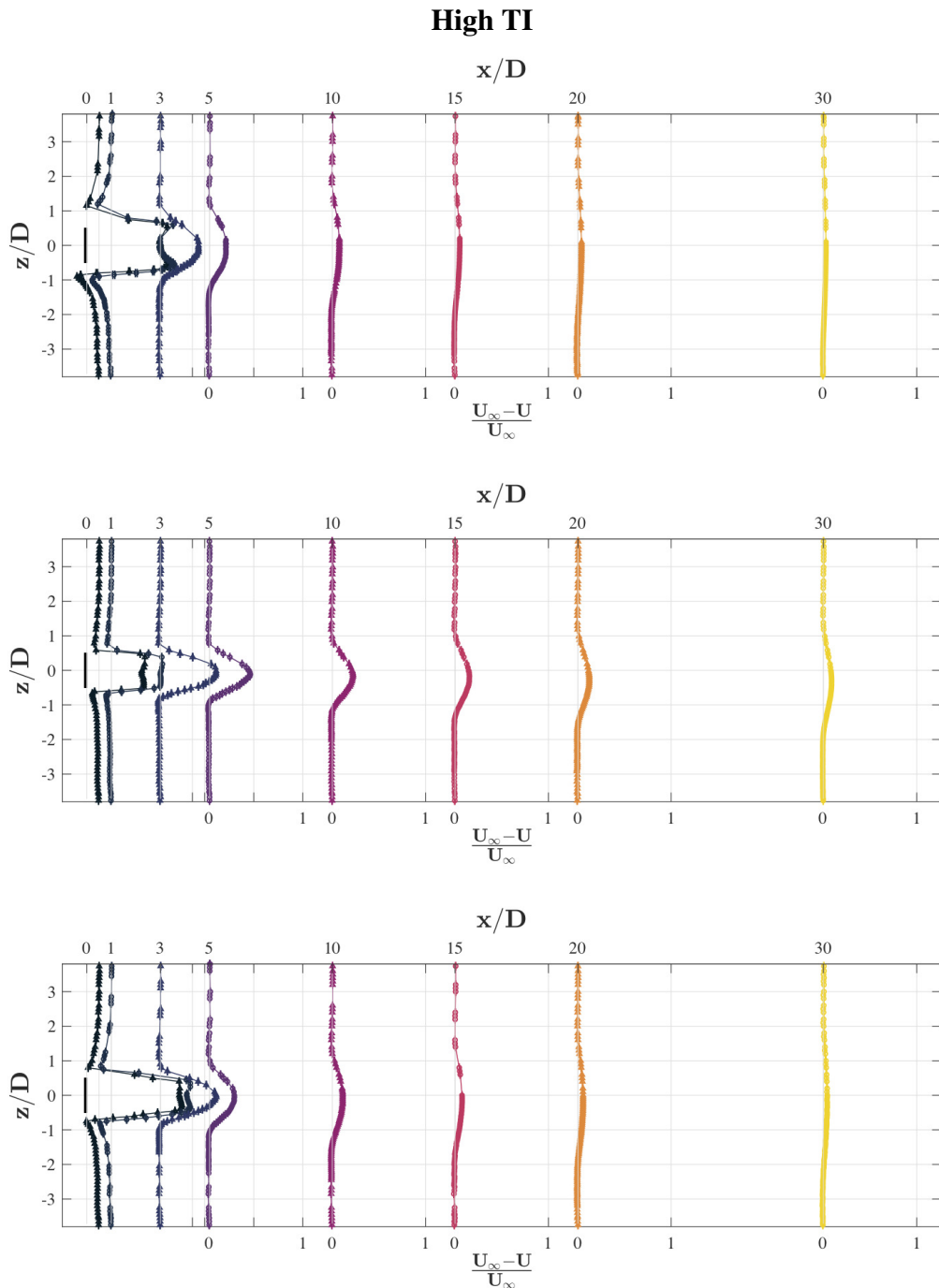


**Figure 3.2:** Mean velocity deficit, an overview of the measurements taken for the turbulent case. From the top: SD, WD and AD. Errorbars indicate statistical uncertainty.

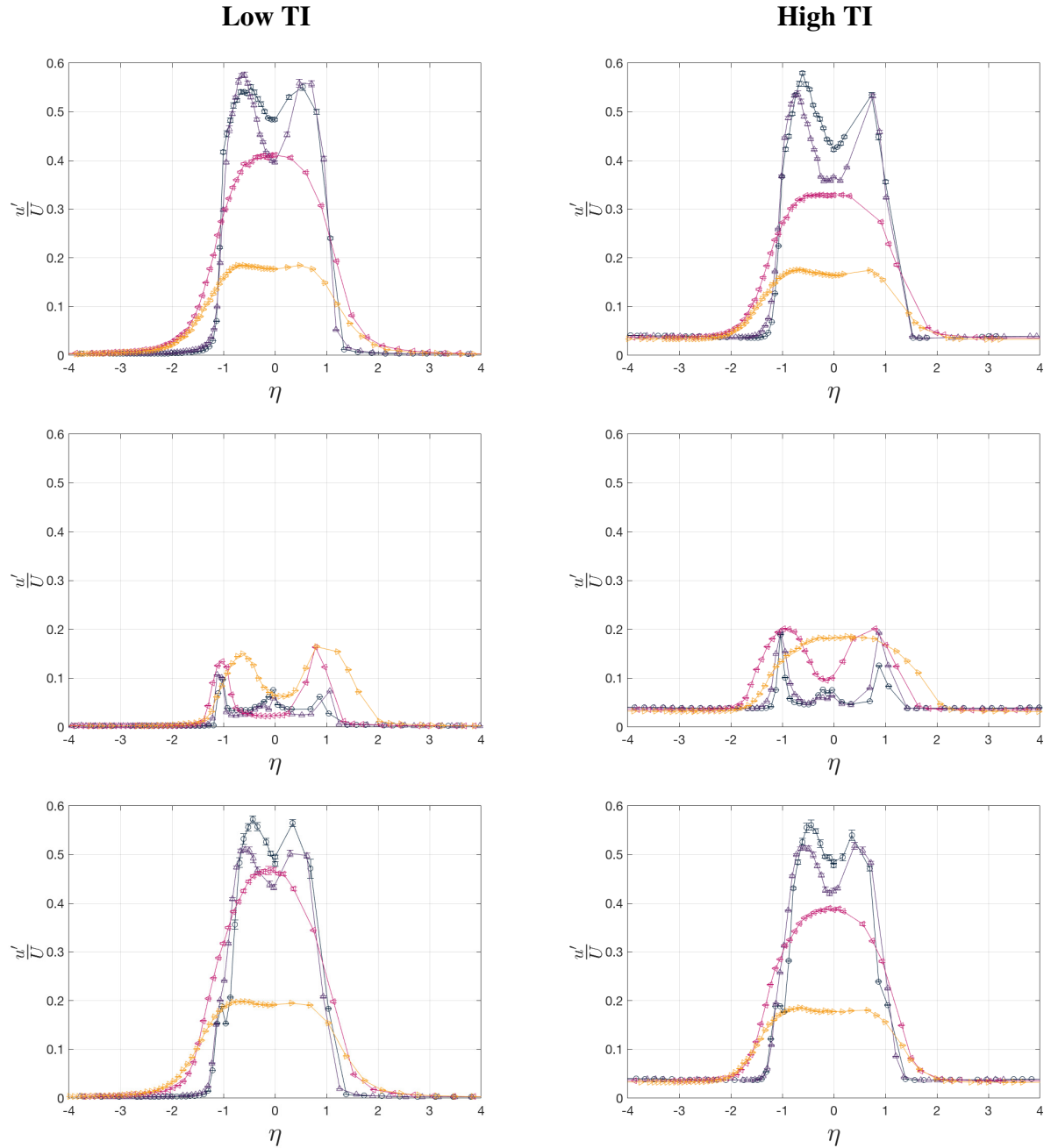


**Figure 3.3:** Turbulence intensity for the near field. Streamwise position is indicated by color, where the darkest is  $x = 0.5D$  and the brightest is  $x = 5D$ . From the top: SD, WD and AD. Errorbars indicate statistical uncertainty.

Figure 3.5a and Figure 3.4 suggest that the wake behind the SD has nearly reached self-similar behaviour already at  $x = 5D$  for the kurtosis in the low incoming turbulence intensity. Looking at the mean velocity, the self-similar behaviour seems prevalent for all disks for both incoming flows downstream of  $x = 5D$ . The power law exponents shown in Table 3.1, are slightly higher than found by Uberoi & Freymuth (1970). However, this is not in contrast to their results, because they found that the self-similar state has established properly first at  $x > 50D$ .

The effect of the tower on the WD is evident close to the disk also in Figures 3.7 and 3.4. For the higher incoming turbulence intensity, the transition to self-similar behaviour appears to be accelerated, this is visible both in Figure 3.5 and Figure 3.6. Rind & Castro (2012a) found that the self-similarity was prevented altogether by the incoming turbulence. Since their investigated domain was  $60 < x/D < 115$ , this can be explained by an overall faster transition to the wake's final state. The increased incoming turbulence appears to speed up the transition to self-similarity and finally to a dissipation of the wake into the freestream flow. The relative uncertainty of the skewness and kurtosis is generally high for the low magnitudes, but the absolute uncertainty is highest in the outer region of the shear layers. In general, the uncertainties are higher for the negative  $z$ -side than the positive. This is expected as the sampling time is much higher in that region. The maximum absolute uncertainties are 0.38 m/s, 0.02, 0.93, and 12.4 for the mean velocity, turbulence intensity, skewness and kurtosis respectively. The near wake is well converged, whereas the outer parts of the shear layer, especially far downstream, is more uncertain. This is discussed more in the appendix.

Another effect of the added turbulence is that the positive peaks in the skewness at the inner edge of the shear layer is completely removed by the higher incoming turbulence. This is the case for all the disks, and is visible in Figure 3.7. In addition, the magnitude of the negative skewness peaks decreases by approximately a factor of 2. The physical meaning of the positive skewness is that the positive fluctuations on average has a higher magnitude than the negative fluctuations and vice versa.

A plausible explanation for the decreasing negative peaks is that the negative gusts occur much more frequently in the high TI case, thereby contributing more to the mean value instead of creating the wide "tails" of the probability distribution.

The kurtosis decreases roughly by a factor of 10 for the high TI case, as can be seen in Figure 3.4. This can be explained by that the fluctuations, both negative and positive, are much more frequent in the high TI flow, and is perhaps the most visible difference between the two flows in Figure 3.8. The fluctuations with the highest absolute magnitude most likely occur for both cases, but since the kurtosis is scaled with  $(\bar{u}^2)^2$  in the denominator, their relative impact on the skewness for whole sample is much smaller for the high TI case.

The effect of turbulence does not seem consistent on the three different disks. As can be seen in Figure 3.9a and 3.9c, the increased turbulence intensity results in faster decay rates of the centre-line velocity, which is in agreement with the findings by Rind & Castro (2012a). However, the onset of the wake recovery of the WD appears to be delayed by the turbulence. Thus, the wake of the WD for the turbulent case would slowly become wider than the wake in the laminar incoming flow if given the space to develop beyond the current domain of  $x/D \leq 30$ , but remains narrower for these experiments. The wake expands considerably slower for the SD and the AD for the higher turbulence intensity, but just barely for the WD.

Table 3.1 and Figure 3.9 illustrate that the velocity deficit decays quite differently for the three disks. Note especially the similarity between the decay rates of the SD and the AD, while the WD has a much slower decay rate. This suggests that the characteristics of the wake created

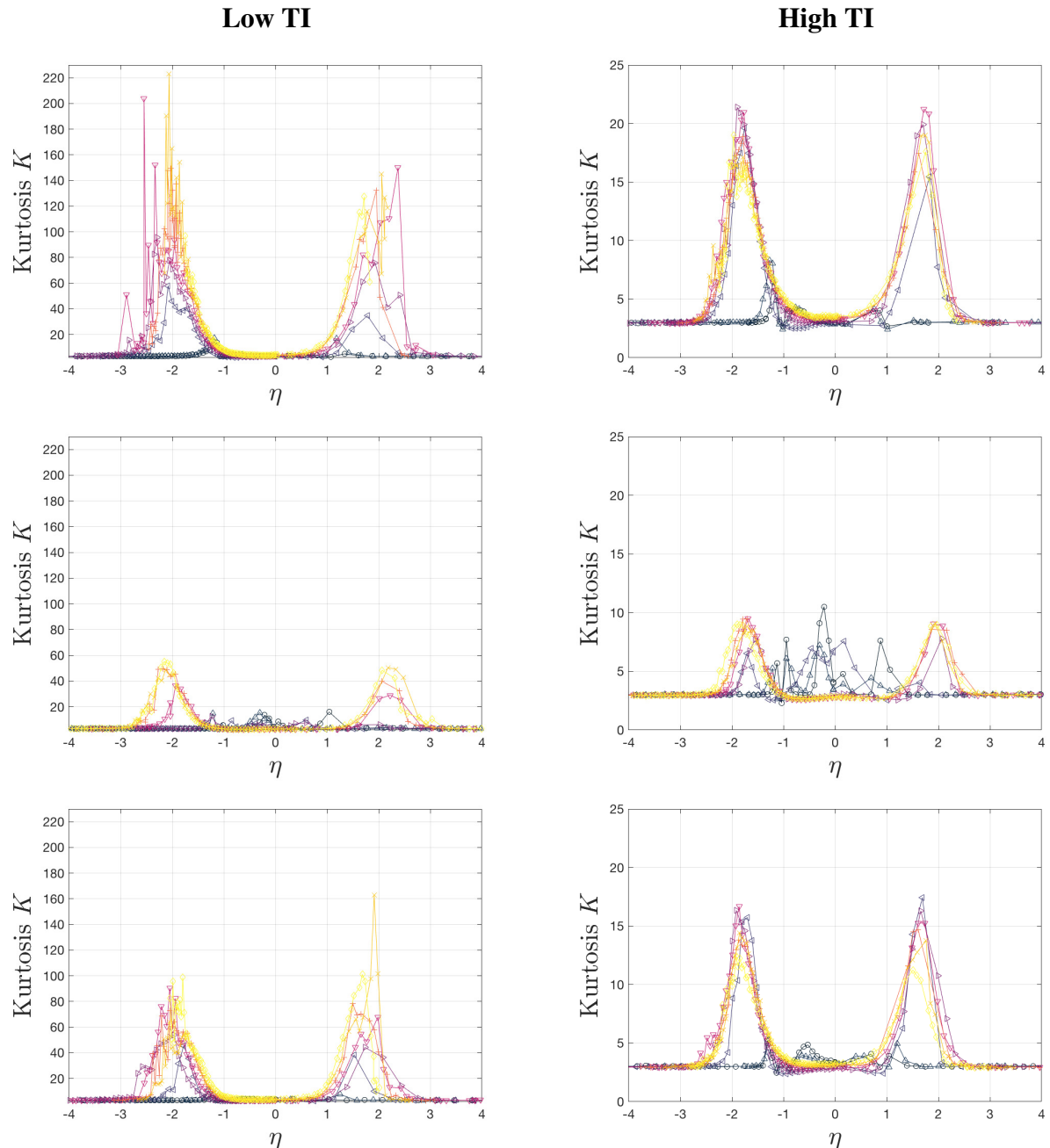


**Figure 3.4:** Kurtosis. Note the different scaling for the two flow regimes. Streamwise position is indicated by color as in Figure 3.7. From the top: SD, WD and AD.

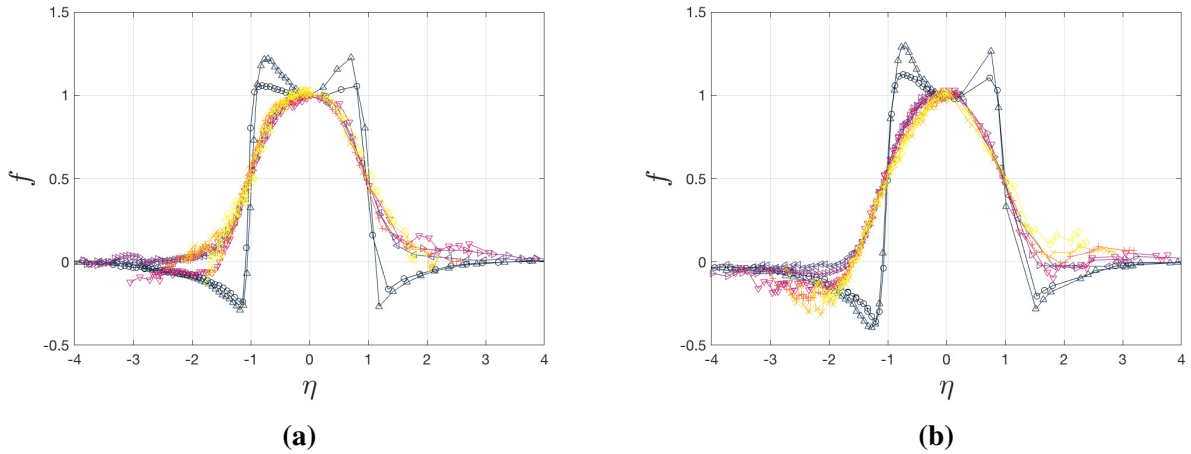


**Figure 3.5:** Self-similarity analysis of the SD. (a) is the low TI case, and (b) is the high TI case. The darkest color is  $x = 0.5D$  and the brightest is  $x = 30D$ .

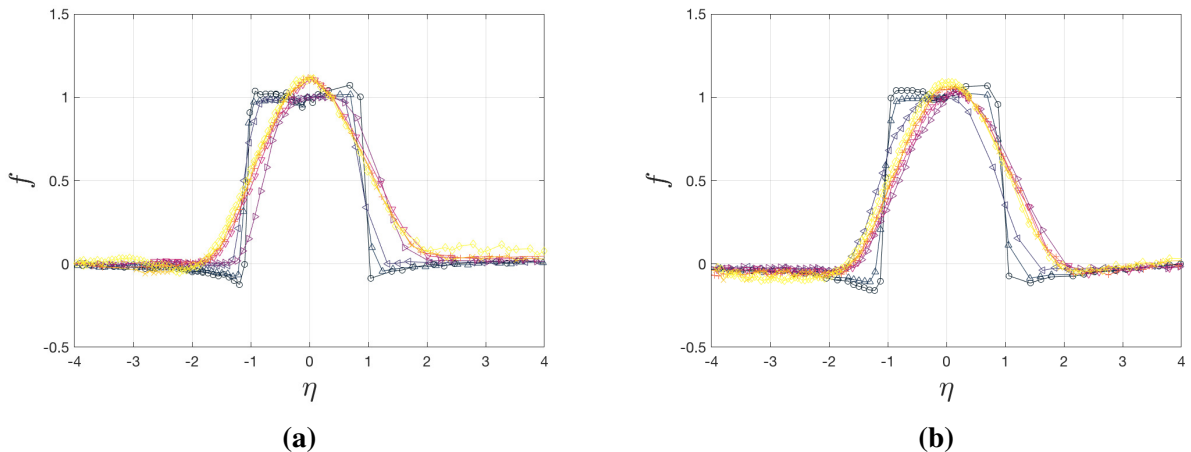


**Figure 3.6:** Self-similarity analysis of the WD.(a) is the low TI case, and (b) is the high TI case. The darkest color is  $x = 0.5D$  and the brightest is  $x = 30D$ .

by a bluff body is indeed dependent on the shape of the body.

It is apparent that the self-similar behaviour appears much earlier for the SD and the AD than for the WD. Since both those disks create much more turbulence, the shear layers meet and interact much earlier than for the WD, so this is consistent.

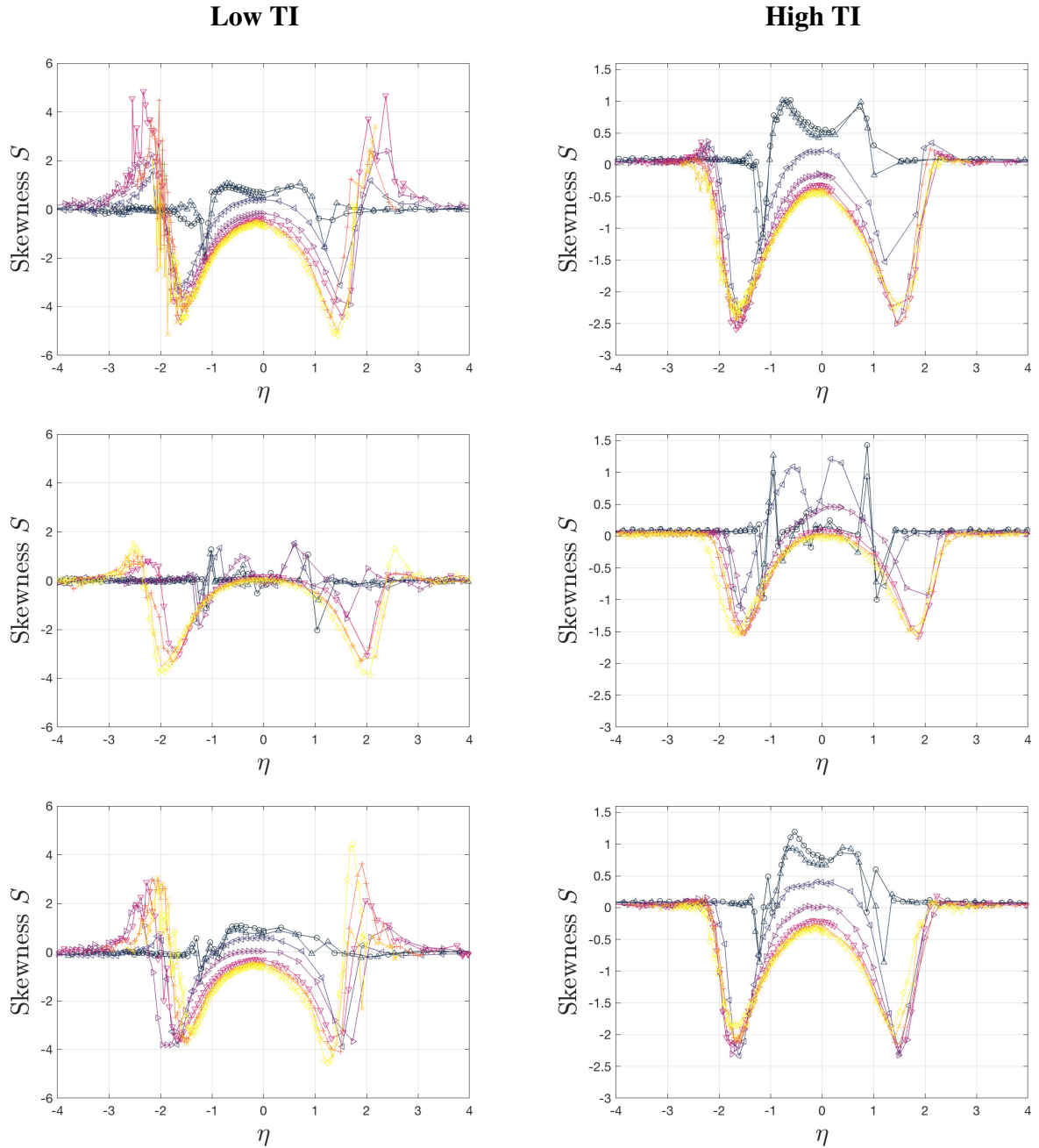


**Figure 3.7:** Skewness. Note the different scaling for the two flow regimes. Streamwise position is indicated by color, where the darkest is  $x = 0.5D$  and the brightest is  $x = 30D$ . From the top: SD, WD and AD.

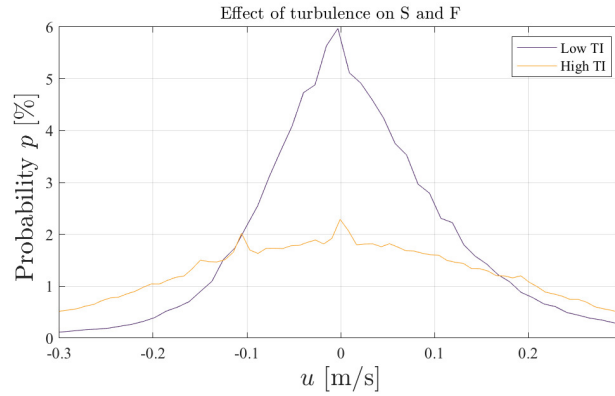


**Figure 3.8:** The probability distribution (PD) compared for the WD at  $\eta = -2.3$  and  $x = 15D$  for the two turbulence intensities. The relevant values for these samples are  $S_L = -3.33$ ,  $S_H = -0.11$ ,  $K_L = 30.27$  and  $K_H = 4.60$ , where subscripts denote low TI and high TI.

**Table 3.1:** Fit coefficients for power laws. For fit quality see figures 3.9 and 3.10.

Disk	Power law for $\delta, n$		Power law for $U_s$	
	Low TI	High TI	Low TI	High TI
SD	0.40	0.37	-0.60	-0.75
WD	0.42	0.33	-0.60	-0.72
AD	0.56	0.34	-0.75	-0.66

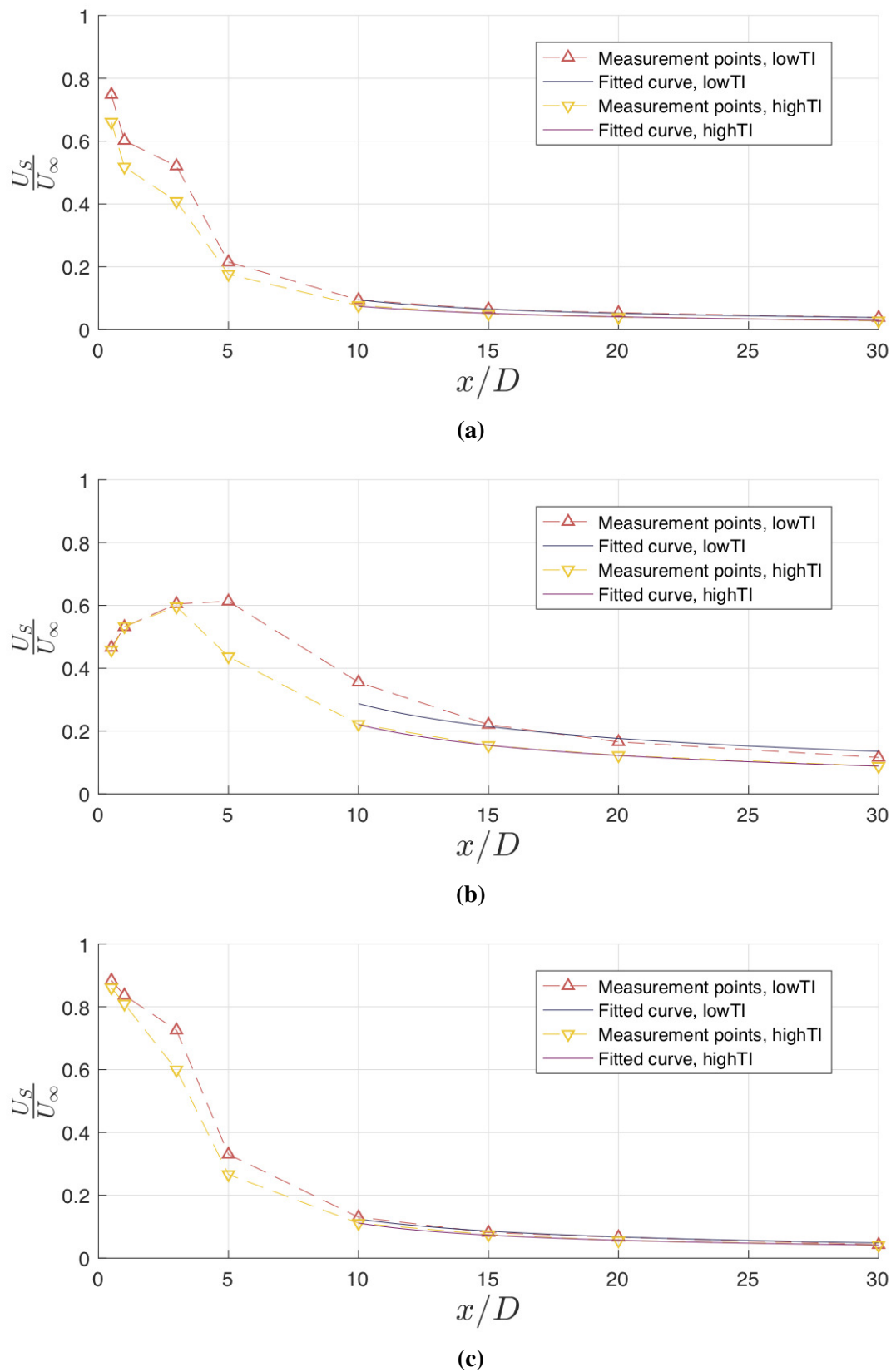


**Figure 3.9:** Power law fits for velocity deficit  $U_S$ . From the top: (a) SD, (b) WD and (c) AD.

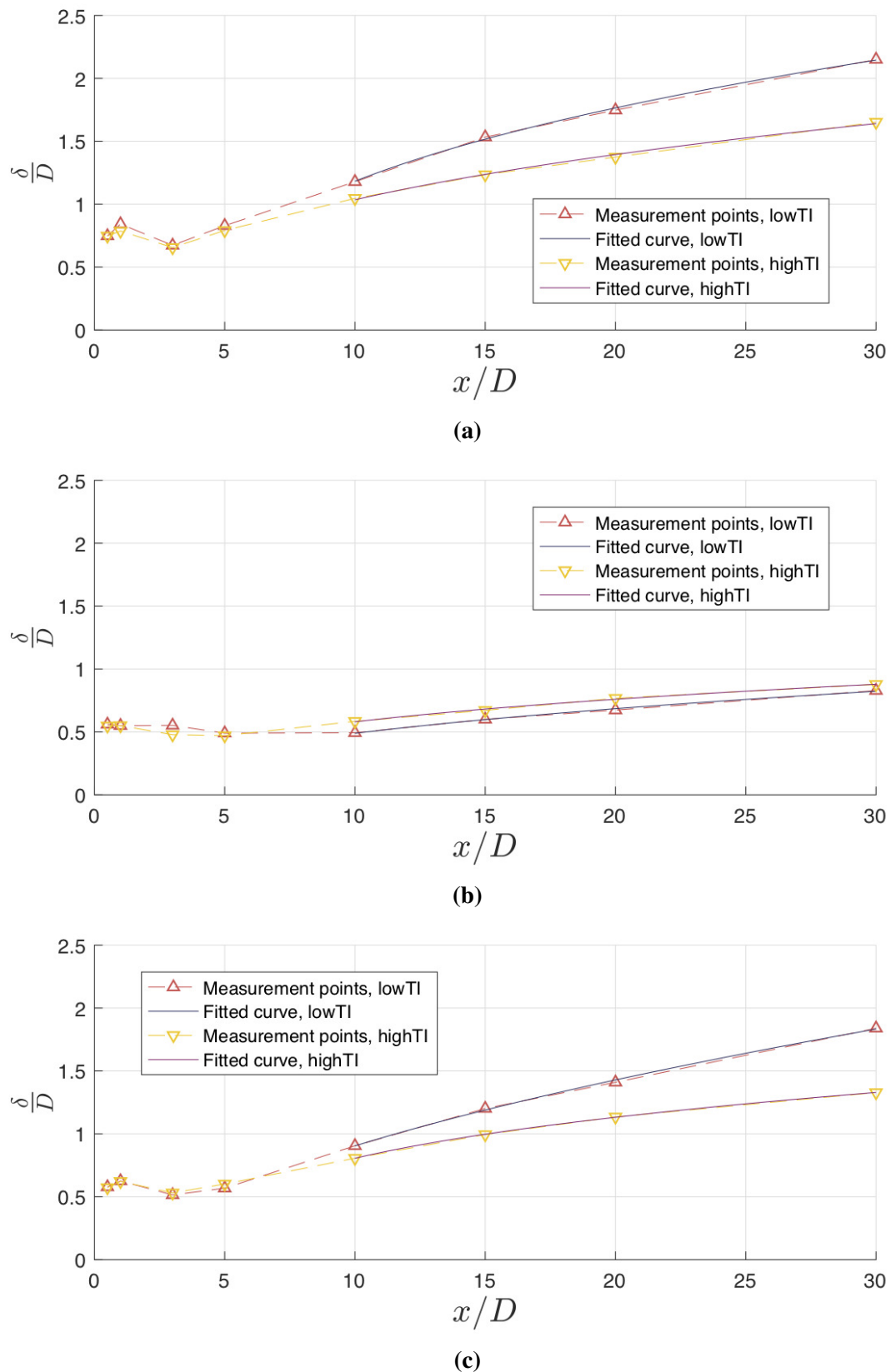


**Figure 3.10:** Power fits for wake half-width  $\delta$ . From the top: (a) SD, (b) WD and (c) AD.



# Chapter 4

## Conclusion

To summarize, a comprehensive study of the wakes behind three disks has been performed. The properties of the wakes behind a solid disk and two different porous disks with the same solidity have been examined through wind tunnel experiments and compared for two incoming turbulence intensities. The aim was to quantify up to fourth order statistics of the wakes and to determine how a perforated disk and a mesh disk compare regarding properties of the wake, and how a change in incoming turbulence intensity affects this. It was found that the higher incoming turbulence decreases the rate of wake half-width decay  $\delta$  and increases the rate centre-line velocity decay  $U_s$  for all disks. The skewness has in general been found to decrease in magnitude in the shear layer by the higher incoming turbulence intensity, and the positive peaks in the skewness are virtually removed for the high TI case. The kurtosis also decreases in magnitude in the shear layers. Since both have been used for the same applications, further studies may investigating how their wakes compare for different turbulent length scales and a bigger range of turbulence intensities. In addition, since wind- and tidal turbines are relevant applications, a more thorough analysis of vortex frequencies would be of interest due to the challenges turbines face regarding fatigue.



# Bibliography

- Aubrun, S., Espa  a, G., Loyer, S., Hayden, P. & Hancock, P. (2012), Is the actuator disc concept sufficient to model the far-wake of a wind turbine?, in M. Oberlack, J. Peinke, A. Talamelli, L. Castillo & M. H  lling, eds, ‘Progress in Turbulence and Wind Energy IV’, Springer Berlin Heidelberg, Berlin, Heidelberg, pp. 227–230.
- Aubrun, S., Loyer, S., Hancock, P. & Hayden, P. (2013), ‘Wind turbine wake properties: Comparison between a non-rotating simplified wind turbine model and a rotating model’, *Journal of Wind Engineering & Industrial Aerodynamics* **120**(C), 1–8.
- Benedict, L. H. & Gould, R. D. (1996), ‘Towards better uncertainty estimates for turbulence statistics’, *Experiments in Fluids* **22**(2), 129–136.  
**URL:** <https://doi.org/10.1007/s003480050030>
- Blackmore, T. (2013), Grid generated turbulence and actuator disc representations of tidal turbines, PhD thesis, University of Southampton.
- Blackmore, T., Batten, W. M. J., M  ller, G. U. & Bahaj, A. S. (2013), ‘Influence of turbulence on the drag of solid discs and turbine simulators in a water current’, *Experiments in Fluids* **55**(1), 1637.  
**URL:** <https://doi.org/10.1007/s00348-013-1637-9>
- Bossuyt, J., Howland, M., Meneveau, C. & Meyers, J. (2017), ‘Measurement of unsteady loading and power output variability in a micro wind farm model in a wind tunnel’, *Experiments in Fluids* **58**(1), 1–17.
- Camp, E. H. (2018), Wind Energy and Wind-Energy-Inspired Turbulent Wakes: Modulation of Structures, Mechanisms and Flow Regimes, PhD thesis, Portland State University.
- Cannon, S. and Champagne, F. G. A. (1993), ‘Observations of large-scale structures in wakes behind axisymmetric bodies’, *Experiments in Fluids* **14**(6), 447–450.  
**URL:** <https://doi.org/10.1007/BF00190199>
- Chevray, R. (1968), ‘The turbulent wake of a body of revolution’, *Journal of Basic Engineering* **90**(2), 275–284.
- Espa  a, G., Aubrun, S., Loyer, S. & Devinant, P. (2012), ‘Wind tunnel study of the wake meandering downstream of a modelled wind turbine as an effect of large scale turbulent eddies’, *Journal of Wind Engineering and Industrial Aerodynamics* **101**, 24 – 33.  
**URL:** <http://www.sciencedirect.com/science/article/pii/S0167610511002157>

## BIBLIOGRAPHY

---

- Higuchi, H., Zhang, J., Furuya, S. & Muzas, B. K. (1998), ‘Immediate and near wake flow patterns behind slotted disks’, *AIAA journal* **36**(9), 1626–1634.
- Hultmark, M. & Smits, A. J. (2010), ‘Temperature corrections for constant temperature and constant current hot-wire anemometers’, *Measurement Science and Technology* **21**(10), 105404.  
**URL:** <http://stacks.iop.org/0957-0233/21/i=10/a=105404>
- Johansson, P. B. V., George, W. K. & Gourlay, M. J. (2003), ‘Equilibrium similarity, effects of initial conditions and local reynolds number on the axisymmetric wake’, *Physics of Fluids* **15**(3), 603–617.  
**URL:** <https://doi.org/10.1063/1.1536976>
- Mohamed, M. S. & Larue, J. C. (1990), ‘The decay power law in grid-generated turbulence’, *Journal of Fluid Mechanics* **219**, 195–214.
- Myers, L. & Bahaj, A. (2010), ‘Experimental analysis of the flow field around horizontal axis tidal turbines by use of scale mesh disk rotor simulators’, *Ocean engineering* **37**(2-3), 218–227.
- Nedic, J. (2013), Fractal-generated wakes, PhD thesis, Imperial College London.
- Pope, S. B. (2000), *Turbulent Flows*, Cambridge University Press.
- Redford, J. A., Castro, I. P. & Coleman, G. N. (2012), ‘On the universality of turbulent axisymmetric wakes’, *Journal of Fluid Mechanics* **710**, 419–452.
- Rind, E. & Castro, I. (2012a), ‘On the effects of free-stream turbulence on axisymmetric disc wakes’, *Experiments in Fluids* **53**(2), 301–318.
- Rind, E. & Castro, I. P. (2012b), ‘Direct numerical simulation of axisymmetric wakes embedded in turbulence’, *Journal of Fluid Mechanics* **710**, 482–504.
- Sforza, S. P. & Smorto, M. (1981), ‘Three-dimensional wakes of simulated wind turbines’, *AIAA Journal* **19**(9), 1101–1107.
- Tennekes, H. & Lumley, J. L. (1972), *A First Course in Turbulence*, The MIT Press.
- Theunissen, R. & Worboys, R. (2019), ‘Near-wake observations behind azimuthally perforated disks with varying hole layout and porosity in smooth airstreams at high reynolds numbers’, *Journal of Fluids Engineering* **141**(5), 051108.
- Townsend, A. (1980), *The Structure of Turbulent Shear Flow*, Cambridge Monographs on Mechanics, Cambridge University Press.
- Uberoi, M. S. & Freymuth, P. (1970), ‘Turbulent energy balance and spectra of the axisymmetric wake’, *The Physics of Fluids* **13**(9), 2205–2210.  
**URL:** <https://aip.scitation.org/doi/abs/10.1063/1.1693225>
- Wu, Y.-T., Liao, T.-L., Chen, C.-K., Lin, C.-Y. & Chen, P.-W. (2019), ‘Power output efficiency in large wind farms with different hub heights and configurations’, *Renewable Energy* **132**, 941 – 949.  
**URL:** <http://www.sciencedirect.com/science/article/pii/S0960148118310012>

- Wu, Y.-T. & Porté-Agel, F. (2012), ‘Atmospheric turbulence effects on wind-turbine wakes: A les study’, *Energies* **5**(12), 5340–5362.  
**URL:** <http://dx.doi.org/10.3390/en5125340>

## *BIBLIOGRAPHY*

---

# Appendix

In order to compensate the hotwires for inter-wire drift, the wires were normalized against wire 1, since this wire was the most reliable during experiments. An example is shown in Figure 4.1.

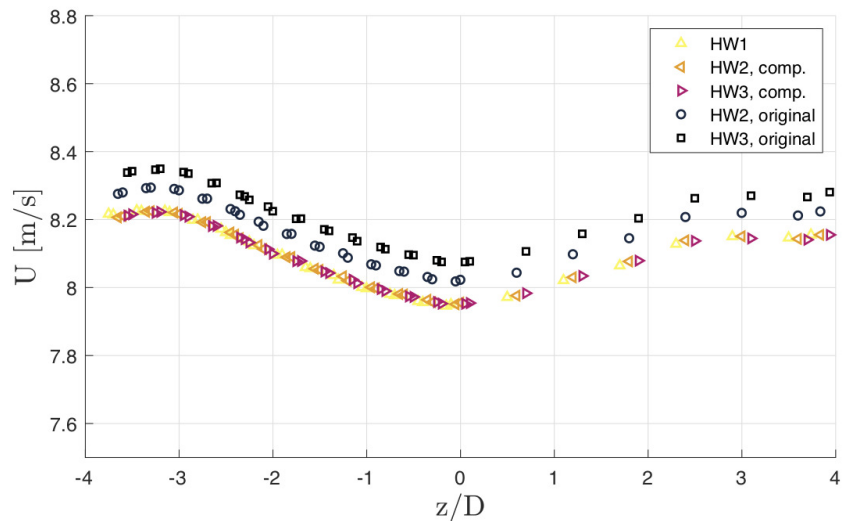


**Figure 4.1:** Wire compensation example. Wire 2 and 3 are multiplied by ratios so that the velocity matches that of wire 1 at the positions where they measure the same flow. This example is from the SD, high TI case at  $x = 30D$ .

In order to determine the filtering frequency and the sampling rate for the experiments, the power spectral density function shown in Figure 4.2 was computed. The figure illustrates the turbulence energy cascade in the most turbulent position measured, and the turbulent energy clearly levels out at 10 kHz, where the filtering frequency was set. All of the signal above this frequency was deemed to be noise.

The probability distribution shown in Figure 4.3 with corresponding values listed in Table 4.1 show a comparison between an original sample, and a sample digitally filtered at a cutoff-frequency of  $f_c = 10$  Hz. What this shows is that the low and high frequency eddies have different probability distributions, where the skewness of the higher frequencies has a much higher magnitude than the low frequencies.

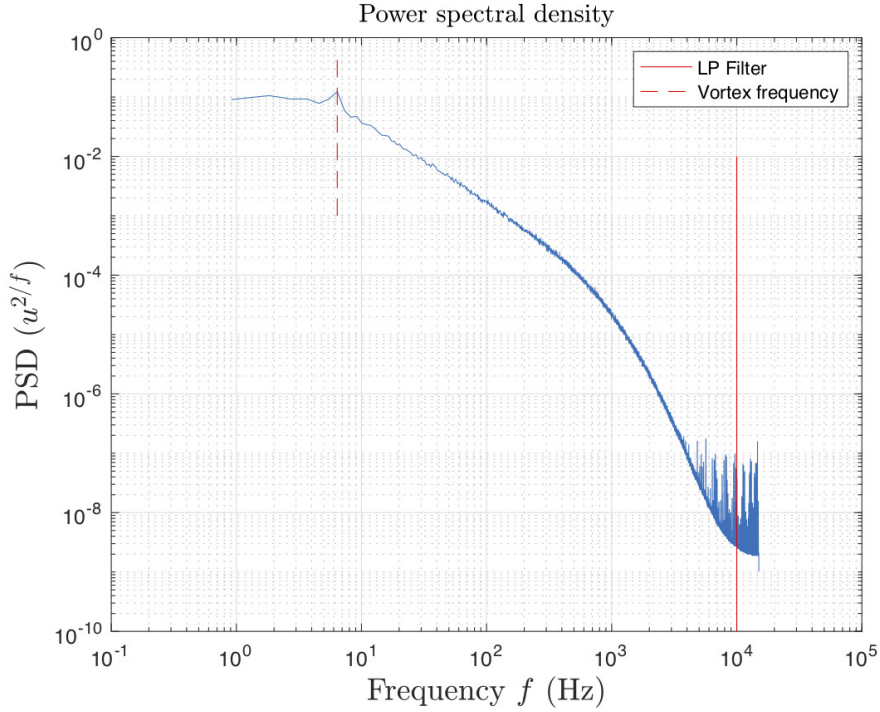


**Figure 4.2:** This sample is taken in the middle of the shear layer at  $x = 0.5D$  downstream of the SD. Note the vortex shedding frequency at 6.4 Hz.

**Table 4.1:** Skewness and kurtosis for the signals shown in Figure 4.3.

	S	F
Original sample	-3.33	30.27
High frequency part	-3.19	20.87
Low frequency part	-1.33	19.15

The error-bars in Figures 4.4 and 4.5 denote statistical uncertainty. The two figures illustrate that the intermittency of the shear layer at the edge is much higher for the SD than the other two disks, as the uncertainties are much higher for the SD. It is clear that even longer sampling times should be used for further studies of perforated disks and solid disks, if high order statistics are to be studied.

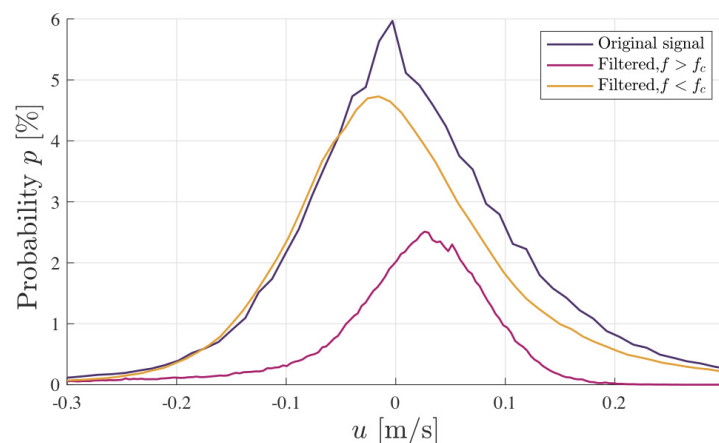


**Figure 4.3:** Comparison of the probability distributions for a sample with the laminar incoming flow at  $\eta = -2.3$  and  $x = 15D$  shown in Figure 3.8 with a spectral lowpass filter applied at a  $f_c = 10$  Hz.

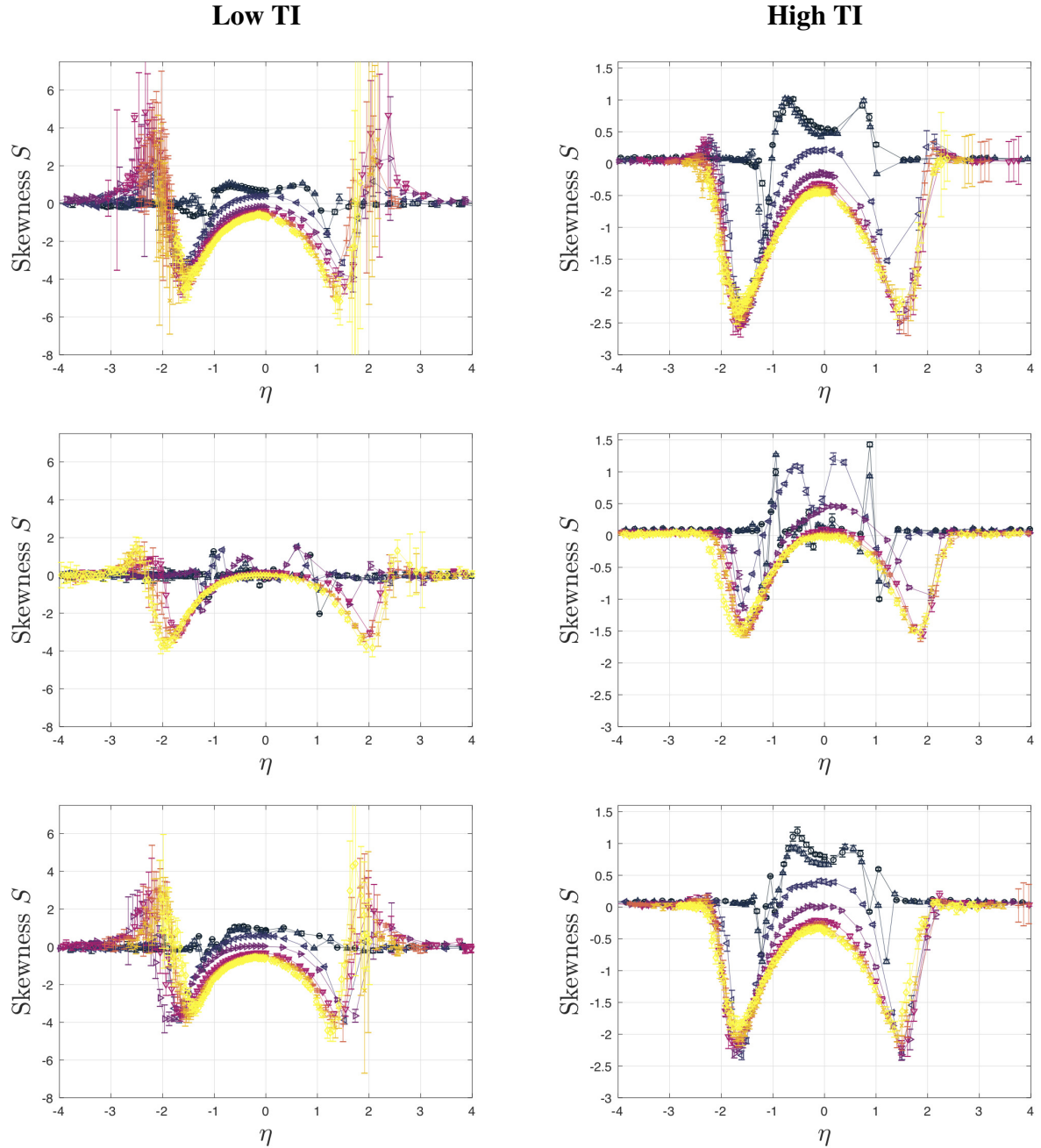


**Figure 4.4:** Skewness. Note the different scaling for the two flow regimes. Streamwise position is indicated by color, where the darkest is  $x = 0.5D$  and the brightest is  $x = 30D$ . From the top: SD, WD and AD.

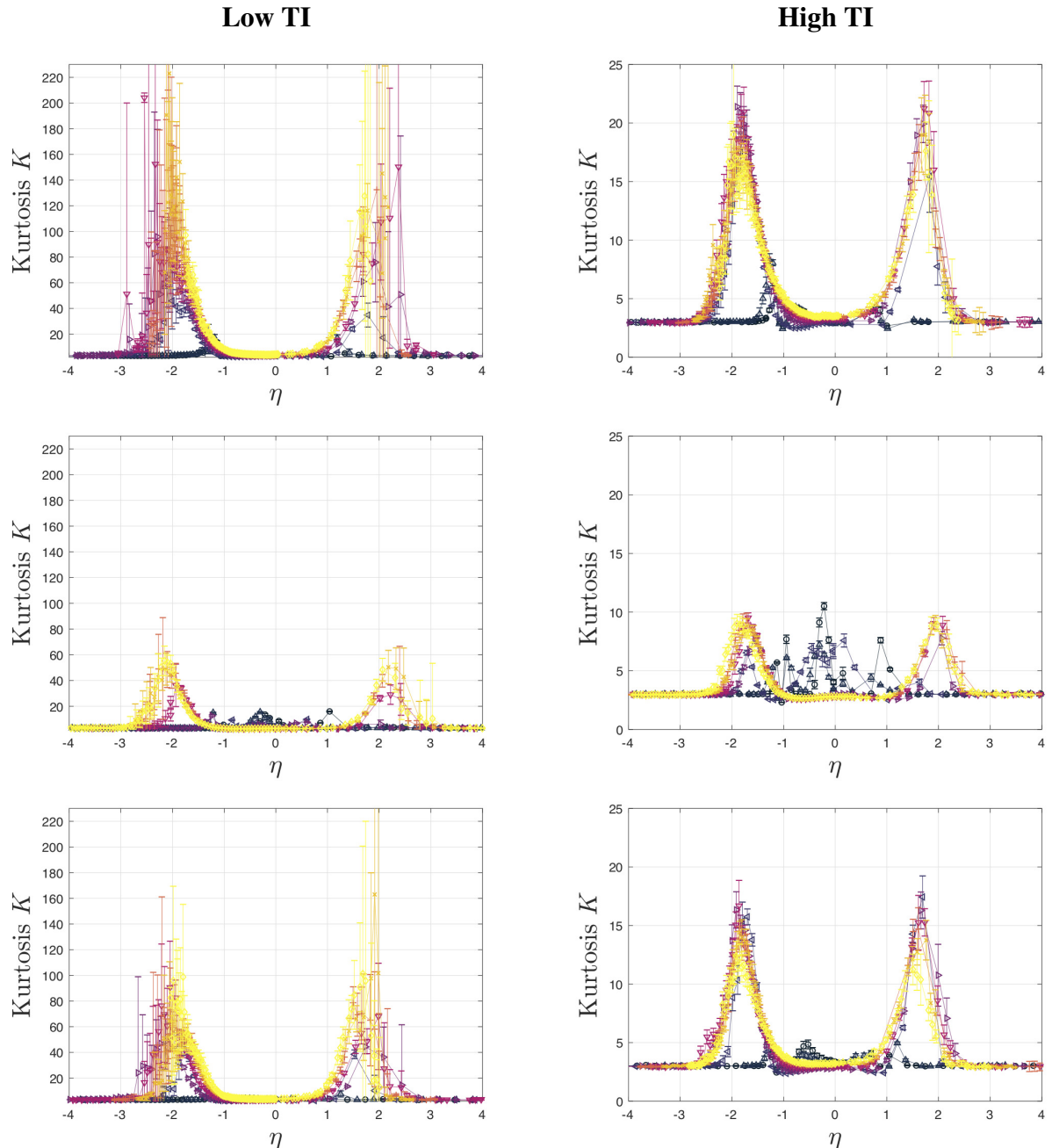


**Figure 4.5:** Kurtosis. Note the different scaling for the two flow regimes. Streamwise position is indicated by color as in Figure 4.4. From the top: SD, WD and AD.